Direct Numerical Simulations of Fundamental Turbulent Flows with the Largest Grid Numbers in the World and its Application of Modeling for Engineering Turbulent Flows

Project Representative
Chuichi Arakawa Graduate School of Interdisciplinary Information Studies, the University of Tokyo

Authors
Chuichi Arakawa *1, Makoto Iida *2, Yukio Kaneda *3, Takashi Ishihara *3, Hiroshi Kawamura *4, Yoshinobu Yamamoto *3, Toshiyuki Gotoh *5 and Takeshi Watanabe *5

*1 Graduate School of Interdisciplinary Information Studies, the University of Tokyo
*2 Graduate School of Engineering, the University of Tokyo
*3 Graduate School of Engineering, Nagoya University
*4 Department of Mechanical Engineering, Tokyo University of Science
*5 Graduate School of Engineering, Nagoya Institute of Technology

In order to understand the statistics and physics of turbulence, we performed large-scale direct numerical simulations (DNS's) of canonical incompressible turbulent flows on the Earth Simulator, including those of (i) turbulence in a periodic box, (ii) multi-phase turbulent shear flows, (iii) turbulent Ekman boundary layer, and (iv) passive scalar turbulence. The DNS data were analyzed to study (i) the energy transfer in the inertial subrange and the multifractal characteristics in fully developed turbulence, (ii) surface deformation effects on turbulence structures for two different types of air-liquid interface turbulent shear flows, (iii) Reynolds number dependence and the three dimensional characteristics in the turbulent Ekman boundary layer, and (iv) the universality of passive scalar turbulence.

We also performed numerical simulations of turbulent flows on the ES from the viewpoint of engineering applications. We made simulation of flows and acoustic fields around horizontal-axial-type of wind turbine by using compressible Large-Eddy Simulation (LES) and direct prediction method of noise, with emphasis on the blade tip region. Aerodynamic performance and acoustic emissions are predicted for the actual tip shape, an ogee type tip shape and an attached winglet. These giant simulations are found to be available for the engineering topics such as design of wind turbine.

Keywords: incompressible turbulence, high-resolution DNS, multi-phase turbulent shear flows, turbulent Ekman boundary layer, passive scalar turbulence, LES, wind turbine, noise reduction

1. Data analyses based on high-resolution DNS of incompressible turbulence

In order to study universal nature of fully developed turbulence at high Reynolds number, we performed data analyses based on DNS of forced incompressible turbulence in a periodic box with the number of grid points up to 4096^3 on the Earth Simulator (ES) [1, 2]. The DNS data have potential ability to elucidate the universal nature of high Reynolds number turbulence. Here we present some results obtained by the recent analyses.

1.1 Energy transfer in the inertial subrange

The statistics of energy transfer $T(k)$ through the wavenumber k was studied by analyzing the data of high resolution DNSs with R_λ up to 1130[2]. The DNSs suggest (i) the PDF of $T(k)$ is far from Gaussian, and it is more intermittent for larger k, (ii) the skewness and flatness factor of the fluctuation of $T(k)$ increases with k, and obey simple scaling laws in the inertial range, and (iii) the volume ratio of backward transfer region is as large as 30–40% (in the use of spectral cut filter) in the inertial subrange.

The statistics of the energy dissipation rate ε and its local volume average ε_r is also studied by using the DNS data. The analysis suggests that in the inertial subrange, (i) the correlation between T and ε_r is not high, but as low as about 0.25, (ii) the locations of intense transfer region and high dissipation region are separated from each other, in contrast to intense forward and backward transfer regions, and (iii) the PDF's of

T and ε_r decreases with $x = (T - \langle T \rangle)/\sigma_T$ or $x = (\varepsilon_r - \langle \varepsilon_r \rangle)/\sigma_{\varepsilon r}$, similarly to each other, for large x, where $\langle a \rangle$ and σ_a denote the average and standard deviation of α, respectively.

The dependence of the statistics of the energy transfer T on the filter function used for the definition of the grid scale component is also studied by comparing the statistics of T_G given by the Gaussian filter with that of T_S given by the spectral cut filter. The volume ratio of backward transfer region for T_G is shown to be smaller than that for T_S, in agreement with previous studies. The moments of T_G are found to scale with k similarly as those of T_S.

1.2 Multifractal analysis

The intermittency of energy dissipation rate ε as well as that of enstrophy Ω in fully developed turbulence, and its scale-similar facets, may be well characterized by using a general formulation in terms of multifractal. In the present study we performed multifractal analysis by using the high-resolution DNS data of turbulence [1, 2], with special emphasis on the similarities and differences between ε and Ω.

In multifractal formulation, the so-called "generalized dimension" Dq is given by

$$\sum_i (a_r(\mathbf{x}_i) r^3 / \langle a \rangle L^3)^q \sim (r/L)^{(q-1)D_q}$$

as a r -independent exponent, where a_r is the average of $a = \varepsilon$, Ω. over a cubic domain of size r around location $\mathbf{x}_i$, and $\langle a \rangle$ is the average of a over a cubic domain of size L in the DNS field. Our preliminary analysis suggests that almost r -independent D_q is obtained for r in the inertial subrange of turbulence obtained by high-resolution DNS and also suggests that the value of D_q for ε agrees well with that for Ω provided that r is in the inertial subrange.

2. DNS of multiphase turbulent shear flows

To investigate surface deformation effects on turbulence structures for two different types of air-liquid interface turbulent shear flows, direct numerical simulations by using the MARS method [3] were performed. One flow filed is a fully-developed wind-driven turbulent flow at maximum wind speed of 2.2 m/s. The other one is an air-liquid counter current flow induced by a high-speed liquid film:"Super-critical turbulent open-channel flow" at Froude number of 1.8 based on the bulk mean velocity and wave velocity of long wave. Instantaneous free-surface behavior for wind-driven flow and super-critical open-channel flow is shown in Fig. 1-(a) and (b), respectively.

In the wind-driven flow, some wind-waves with the crests are observed and wind-waves are formed to the large scale-shapes in the horizontal directions. On the other hands, in the super-critical open-channel flow, gently bumped waves and high-frequency fluctuations on them are observed.

Figures 2 and 3 show pressure-strain term distribution, where φ_{11}, φ_{22}, φ_{33} denotes streamwise, vertical and spanwise pressure-strain term, respectively. Nevertheless flow type difference, the redistribution from the vertical pressure-strain term to others is dominant during the surface deformation range. But, the spanwise pressure-strain term contribution is bigger and reverses the vertical value at the vicinity of the air-liquid interface ($y^+ > 160$) in wind-driven

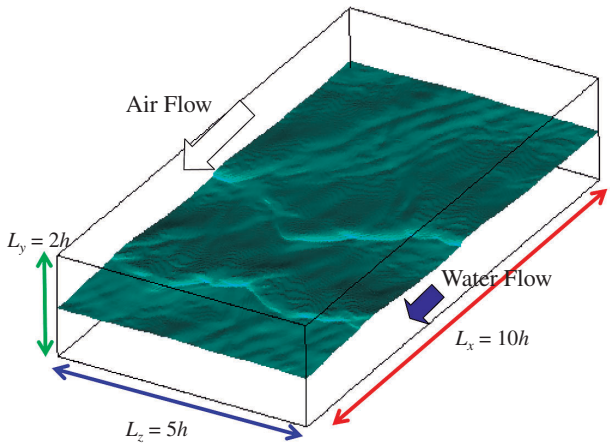

(a) Wind-driven turbulent flow

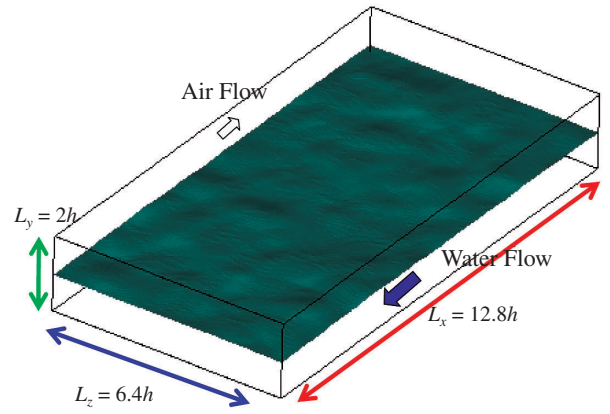

(b) Super-critical turbulent open-channel flow

Fig. 1 Instantaneous free-surface behaviors.

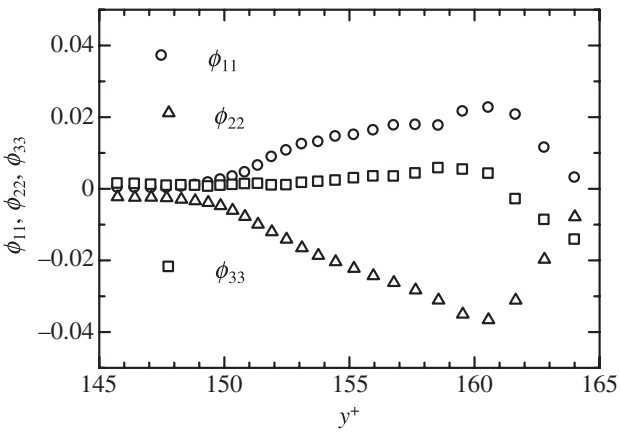

Fig. 2 Pressure-strain term distributions, water side. (Wind-driven flow)

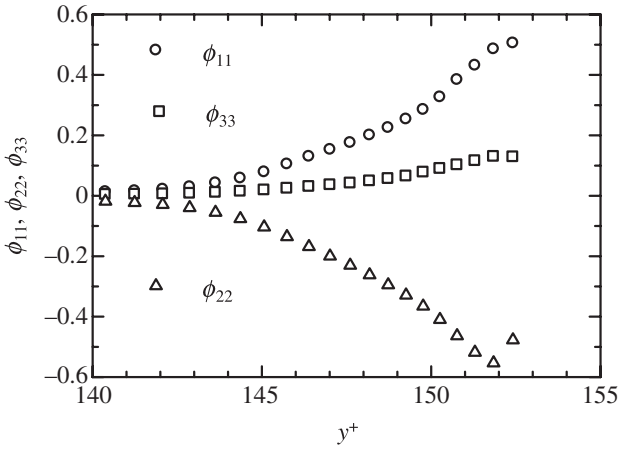

Fig. 3 Pressure-strain term distributions, water side. (Super-critical open-channel flow)

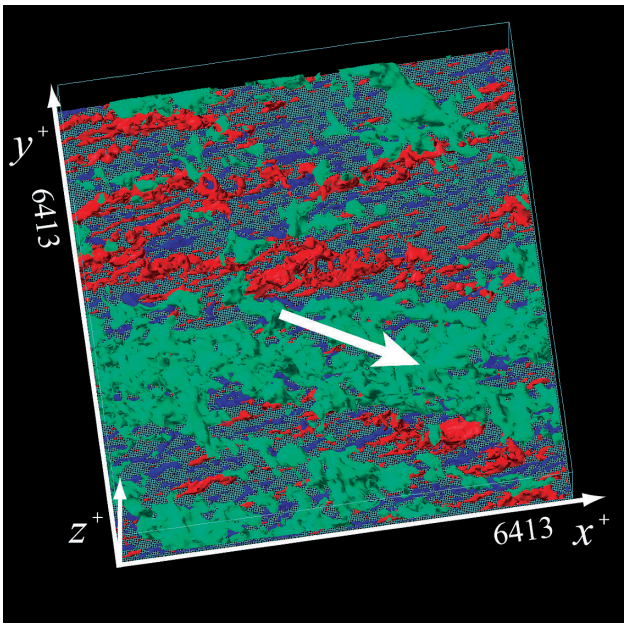

Fig. 4 Bird's eye view of instantaneous flow field for Re_f = 1393. Red, high-speed regions $u'^+ > 3.0$; blue, low-speed regions $u'^+ < -3.0$; green, low-speed regions in the upper region $u'^+ < -1.2$ at $z/D > 5$ where D is the viscous Ekman layer depth.

flow. Because, free-surface acts as a kind of wall in wind-driven flow and high-frequency free-surface deformation itself causes turbulence in super-critical open-channel flow. These pressure-strain terms behaviors support well turbulent intensity distribution near free-surface for each case and free-surface turbulent model would be required to satisfy these characteristics.

3. DNS of the turbulent Ekman boundary layer

Rotation is one of the factors which affect the planetary boundary layer (PBL). The boundary layer under the effect of the system rotation is called the Ekman boundary layer. The Ekman boundary layer is three-dimensional flow in nature, in which three forces are balanced, i.e., the pressure gradient, viscous and the Coriolis forces.

In the present study, we calculated DNSs of the neutrally stratified turbulent Ekman boundary layer up to the Reynolds numbers of Re_f = 1393 where Re_f is based on the geostrophic wind, the kinematic viscosity and Coriolis parameter. Our objective is to investigate Reynolds number dependence and the three-dimensional characteristics in the turbulent Ekman boundary layer. The Reynolds number attainable through DNS is, however, still much smaller than those of the actual PBL. The RANS plays an important role in the simulation of the PBL. Accordingly, we evaluate the eddy-viscosity model [4] to improve it based on the present results.

A bird's eye view of an instantaneous flow field is displayed in Fig. 4 to grasp the three-dimensional characteristics of the turbulence structures. The streaky structures are observed near the wall and elongated along the mean velocity direction. On the other hand, large low-speed regions exist in the upper region. The large-scale structures rise up from the bottom because the low-speed fluid is conveyed from the bottom wall. The structures are not aligned in the direction of the mean velocity. They are elongated approximately in the direction of the geostrophic wind (in the x-direction) and are also inclined slightly toward the higher pressure side (in the minus y-direction).

Many theoretical approaches to the turbulent Ekman problem have employed some empirical specification for the eddy-viscosity. Among them, we examine a mixing length model [4] in comparison with the present DNS data. An improvement is also proposed to the expression of the mixing length. We introduce the viscous effect in the near wall region and accommodate an empirical parameter relevant to the upper region. The present model predicts the mean velocity profiles give a much better agreement with the DNS data (not shown here).

4. DNS of passive scalar turbulence under the uniform mean scalar gradient

Universality in turbulence has long been a central issue in fundamental physics of turbulence since Kolmogorov. The universality of passive scalar turbulence means that when the velocity field at small scales is in an asymptotic statistical state which is independent of large scales, the passive scalar statistics becomes independent of the large scales of both scalar and velocity fields. In order to examine to what extent the universality prevails, it is very effective to change large scale conditions of the scalar alone while keeping the turbulent velocity field the same and to see the difference in the scalar statistics. It is ideal for this purpose to choose the isotropic turbulent velocity field having a well developed scaling range.

We have examined the passive scalar turbulence in 3D by using high resolution DNS [5]. The scalar field is maintained

by two kinds of external sources, a large scale random Gaussian source or a uniform mean scalar gradient. It was found that the scaling exponents of the structure functions of scalar increments in parallel (z axis) and perpendicular (x axis) directions to the mean gradient were the same and saturate about 1.3 at large order, and that they were dependent on scalar injection scheme at large scales within the Reynolds numbers studied.

Figure 5 shows the one-dimensional profiles of the scalar amplitude along z (upper curve) and x (lower one) directions, respectively. Plateaus in $\theta(z) + Gz$, the ramp structure of the integral scale L, appear in z direction, while the structure of θ in x direction is of the form of mesa and canyon. Large jumps in θ at cliffs are of the order of θ_{rms}. Figure 6 shows that the far tails of the probability density functions (PDFs) for the scalar increment in the inertial convective range are well scaled by the saturated scaling exponents and θ_{rms}. These facts suggest that the small scale statistics is to some extent related to the large scales and the universality in passive scalar turbulence should be carefully examined. Studies on the effects of large scale conditions on the small scales with higher resolution are highly indispensable.

5. Numerical approach for aerodynamics and aeroacoustics of wind turbine blade tip

Aerodynamic noise is caused by the rotation of wind turbine blades. Noise prediction and its reduction are essential for wind turbines to spread further, as well as improvement in aerodynamic performance. Especially, high frequency broadband noise increases approximately with the fifth or sixth power of the effective flow velocity of the blade section. Therefore, it is expected to modify and optimize the tip shape.

In numerical simulation, the authors simulated directly the flow and the noise around rotating wind turbine blades with two different tip shapes using compressible Large-Eddy-Simulation (LES)[6]. They succeeded in capturing the complex structure of tip vortices, and showed the effect of the difference between two tip shapes on the aerodynamic noise. Their results showed the similar trend with the experimental measurement.

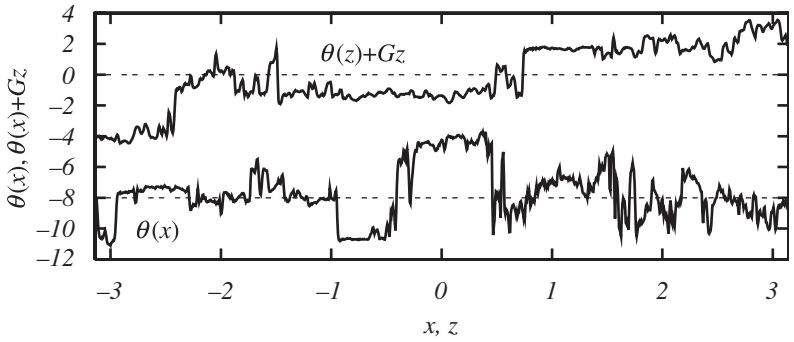

Fig. 5 One dimensional profile of $\theta(z) + Gz$ in z (upper curve) and $\theta(x)$ in x (lower curve) directions, respectively.

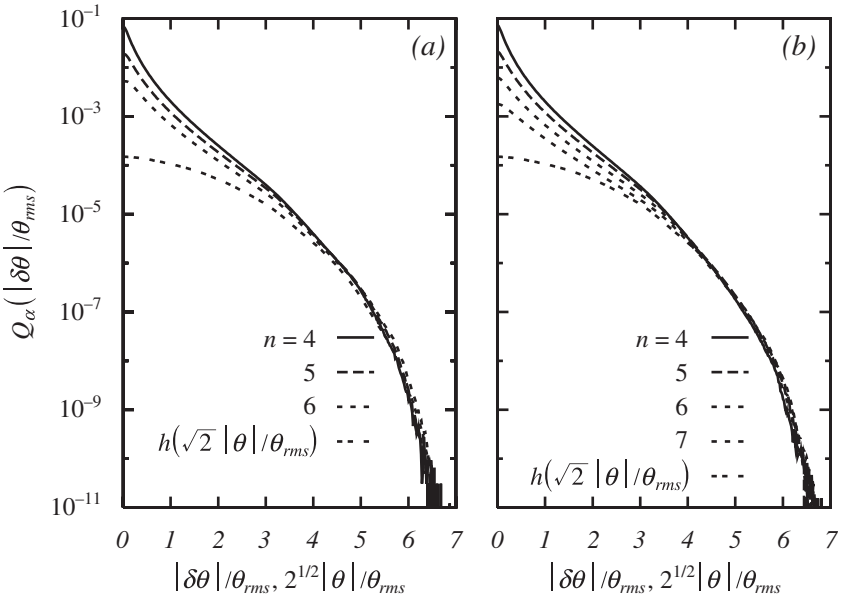

Fig. 6 Scaled PDFs $P_\alpha(|\delta\theta|,r)$ (a) for $\alpha = //$, (b) $\alpha = \perp$. r_n, (n = 4,5,6) is in the inertial range of separation distance.

The aim of this research is to obtain further knowledge of the effect of the blade tip shape on the aerodynamic noise and performance. The winglet is applied for a rotating wind turbine blade tip, and the effect of attached small wing is investigated with the giant numerical simulation of 300 million grid points.

The winglet has been said to diffuse vortices toward the tip, reducing the downwash effects and the induced drag in the three dimensional system of blade. Several researches have existed such as "tip-vanes" and "Mie-vanes" as examples of wind turbine blades. It is found in their experiments that small wings can reduce tip vortices, and make a rotor wake larger. In numerical analysis, van Bussel and Hasegawa have shown that winglets causes some increase in rotor output, using momentum theory and vortex lattice method, respectively. However, these analyses were insufficient to capture 3-dimensional structure of tip vortices as well as aerodynamic noise accurately. Furthermore, the increase of aerodynamic performance has never been based on detailed information of physical phenomena.

In order to capture the three-dimensional structure of tip vortices accurately, we use compressible LES for the flow field, and combine LES with Ffowcs Williams-Hawkings (FW-H) acoustic analogy for the acoustic field. Three types of winglets are simulated for installation angle of 0, 20 and 50 degree.

We have succeeded in capturing differences in the detailed structure of tip vortices among them. These differences were found to cause the overall broadband noise in each level. As for the aerodynamic performance, winglets suppress tip vortices from drifting up to the suction side of the blade, reducing the downwash effects.

Fig. 7 shows the contours of vortices at the near wake of the tip region with their magnitude of iso-surfaces ($|\omega| = 4.0$). Each contoured section corresponds to y/c = 1.0, 1.2, 1.4, 1.6, 1.8, 2.0 where c is chord length and y is distance from the trailing edge. As for 50 deg, the reduction of the strength of tip vortices can be seen at any section, resulting in larger dissipation for 50 deg than for 0 deg near the wall. It is confirmed that winglets surely make vortices weak near the tip region.

As shown in Fig. 8, the pressure fluctuations are observed at the two points, *Point A* and *Point B*, which are located slightly downstream of the blade trailing edge, i.e., 50 grid points away from the blade surface. *Point A* is located where the tip vortices are exactly developed, while *Point B* is in the region of the main blade near the winglet. At *Point A*, the power of pressure fluctuations for 50 deg is estimated to be increased for each frequency especially above 4 *kHz*, which comes from the fact that the small-scale structure of tip vortices are strongly induced by the winglet as investigated in Fig. 7. On the other hand, at *Point B*, both estimations for 50 deg and 0 deg are the same order in pressure fluctuation

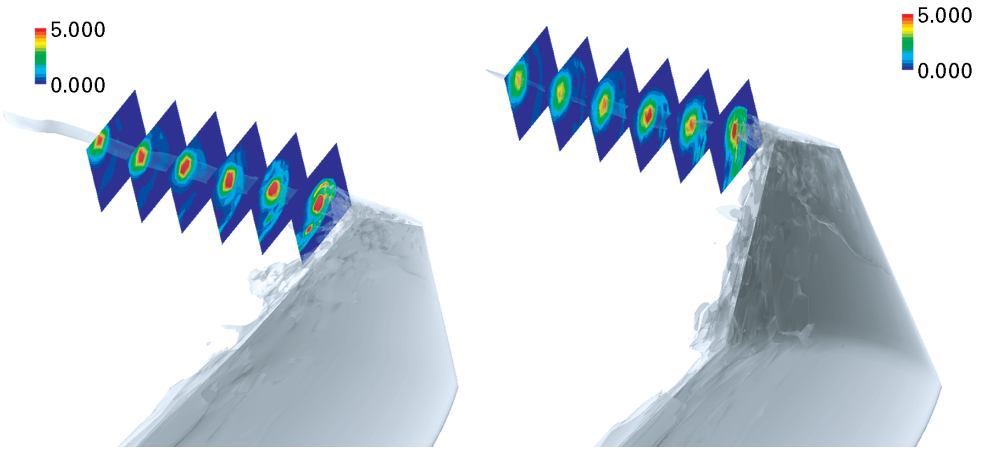

Fig. 7 Color contours of vortices at tip region for standard and winglet rotating blade in wind turbines.

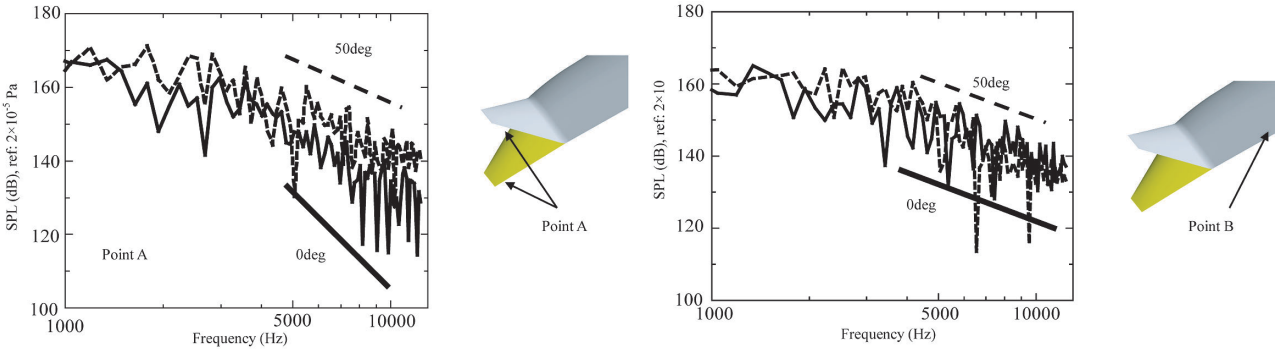

Fig. 8 Pressure fluctuations estimated for standard and winglet rotating blade in wind turbines at two stations.

level. Smaller but more complex structure of tip vortices caused by a winglet can be thought to emit strong noise especially in high frequency.

The performance in aerodynamics is also analyzed and it is confirmed that the winglet clearly improves the efficiency of wind turbines although the detailed information is not described here.

6. Summary

Several basic researches are carried out in direct numerical simulations for turbulent flows where new information are derived and will contribute to the turbulent modeling for applications. In parallel, the application for wind turbines is found to be available for developing new trend of machines in the frame of giant simulation with the Earth Simulator.

References

[1] Y. Kaneda, T. Ishihara, M. Yokokawa, K. Itakura, and A. Uno, "Energy dissipation rate and energy spectrum in high resolution direct numerical simulations of turbulence in a periodic box," Phys. Fluids, vol.15, no.2, pp.L21–L24, 2003.

[2] T. Aoyama, T. Ishihara, Y. Kaneda, M. Yokokawa, K. Itakura, and A. Uno, "Statistics of Energy Transfer in High-Resolution Direct Numerical Simulation of Turbulence in a Periodic Box," J. Phys. Soc. Jpn. vol.74, no.12, pp.3202–3212, 2005.

[3] T. Kunugi, "MARS for multiphse calculation," Comput. Fluid Dynamics J., vol.9, no.1, pp.563–571, 2001.

[4] A. K. Blackadar, "A single-layer theory of the vertical distribution of wind in a baroclinic neutral atmospheric boundary layer," Final Rept. AFCRL-65-531, Pennsylvania State University, pp.22, 1965.

[5] T. Watanabe and T. Gotoh. "Intermittency in passive scalar turbulence under the uniform mean scalar gradient," Submitted to Phys. of Fluids (2005).

[6] C. Arakawa, O. Fleig, M. Iida and M. Shimooka, "Numerical Approach for Noise Reduction of Wind Turbine Blade Tip with Earth Simulator", Journal of the Earth Simulator, Vol.2, pp.11–33, (2005).

乱流の世界最大規模直接計算とモデリングによる応用計算

プロジェクト責任者
荒川　忠一　　東京大学　大学院情報学環

著者
荒川　忠一*1，飯田　　誠*2，金田　行雄*3，石原　　卓*3，山本　義暢*3，河村　　洋*4，
後藤　俊幸*5，渡邊　　威*5

*1　東京大学　大学院情報学環
*2　東京大学　大学院工学系研究科
*3　名古屋大学　大学院工学研究科
*4　東京理科大学　理工学部　機械工学科
*5　名古屋工業大学　大学院工学研究科

乱流の統計と物理を理解するため、地球シミュレータ(ES)を用いて、非圧縮性乱流のいくつかのカノニカルな問題に対する大規模直接数値計算(DNS)とデータの解析を行った。具体的には、(i)最大格子点数4096^3の周期的乱流、(ii)多相せん断乱流、(iii)エクマン境界層乱流、(iv)パッシブスカラー乱流である。(i)では、DNSにより得られたデータを解析した結果、慣性小領域のスケールにおけるエネルギー輸送とそのスケールで平均したエネルギー散逸率の間にある類似性があることを発見した。また、エネルギー散逸率とエンストロフィに着目してマルチフラクタル解析を行った結果、両者の一般化次元等が慣性小領域のスケールで互いに非常によく一致することが分かった。また(ii)では、MARS法を用いた気液境界のせん断乱流のDNSを行い、界面の変形が界面近傍の乱流構造に及ぼす影響について調べた。(iii)ではレイノルズ数1393のエクマン境界層のDNSを実現し、流れ構造を調べるとともに、渦粘性モデルの検証と改良を行い、改良したモデルがDNSとよく一致することを示した。(iv)ではパッシブスカラー乱流の大規模DNSを行い、パッシブスカラー場の小スケールにおける統計が大きいスケールの影響を受けるため、その普遍的な性質を調べる際には注意が必要であることが分かった。

水平軸風車において詳細な空力特性評価を行うことは、より最適な風車翼形状の設計に向けた重要な指針を与える。特に、風車翼端での相対流入速度は、受風面(ロータ面)に流入する風速の8～10倍になり、翼端形状が流れ場及びそれに起因する特性に及ぼす影響も大きい。したがって、翼端形状も含めた、風車翼まわりの流れ場を詳細に解析する必要がある。過去にも、翼端形状を加工することにより風車の騒音低減や、風車性能の向上を目指す研究は多くある。本稿では、翼端形状に着目しつつ、数値シミュレーションにより、風車翼周りの流れ場の詳細解析により空力特性評価を行った。翼端形状には、過去に空力性能向上の報告がなされているウィングレットを採用し、従来型の風車翼との比較を行った。さらに、設計ツールとして応用することを目標に、計算負荷の削減のために格子点数の影響を調査し、実用的な計算規模での評価を行った。

本稿では、翼端渦及び翼近傍の流れ場を、非定常性も考慮した上で詳細に捉えるために、非定常圧縮性LESコードを用いた。本計算コードは著者らが開発してきたコードで、過去に詳細騒音解析の実績を有する。計算は、海洋研究開発機構の地球シミュレータを用いて行った。

この3億点規模の高解像度LES計算により、翼端形状の相違も考慮した翼全体計算を行い、流れ場の詳細解析、及び空力性能評価を行った。本計算により、ウィングレットの空力特性を捉え、過去に報告されてきたウィングレットの効果を検証することができた。これは、翼端付近に格子点を細かく配置し、詳細な渦構造を捉えることを実現した結果であるといえる。

キーワード：非圧縮性乱流，大規模直接数値計算，多相せん断乱流，エクマン境界層，パッシブスカラー場，
ラージ・エディ・シミュレーション，風車，騒音